Matter-wave scattering and guiding by atomic arrays

J. Y. Vaishnav,[1,*] J. D. Walls,[2] M. Apratim,[3] and E. J. Heller[1,2]
[1]*Department of Physics, Harvard University, Cambridge, Massachusetts 02138, USA*
[2]*Department of Chemistry and Chemical Biology, Harvard University, Cambridge, Massachusetts 02138, USA*
[3]*Department of Electrical Engineering, Indian Institute of Technology, Kharagpur 721302, India*
(Received 8 March 2007; published 19 July 2007)

We investigate the possibility that linear arrays of atoms can guide matter waves, much as fiber optics guide light. We model the atomic line as a quasi-one-dimensional array of *s*-wave point scatterers embedded in two-dimensions. Our theoretical study reveals how matter-wave guiding arises from the interplay of scattering phenomena with bands and conduction along the array. We discuss the conditions under which a straight or curved array of atoms can guide a beam focused at one end of the array.

DOI: 10.1103/PhysRevA.76.013620 PACS number(s): 03.75.Lm, 34.50.−s, 68.49.Bc, 72.10.Fk

I. INTRODUCTION

In this paper, we discuss the possibility of using a line of atoms to guide matter waves, such as electrons or other atoms. Periodic arrays often behave as waveguides; perhaps the most familiar example is electrons propagating in a metal. Such waveguides can be engineered as well, such as the guiding of electromagnetic waves in a photonic crystal comprised of aluminum rods (see, e.g., [1]). Although the problem of scattering from periodic arrays is an old one, it arises now in a completely new context, as recent technology allows structures to be engineered from individual atoms. Single chains of Au atoms, for example, have recently been deposited on NiAl(110) [2,3] as well as on Si(553) [4]. Although our formalism does not treat this situation specifically, artificial arrays of atoms also arise when atoms are confined to individual sites in an optical lattices. One might also imagine the individual scatterers being an array of quantum dots, which could be used to guide electrons.

We model the atomic array as a set of *s*-wave scatterers. The question of relevance from an experimental point of view is whether we can use such an atomic array to guide waves. Theoretically, this question translates into whether eigenstates of the system exist which are propagating along but are evanescent transversely to the array. In order to search for these states, we employ scattering theory. Along the array, the system's periodicity gives rise to Bloch waves, band structure, diffraction, and other features familiar from solid-state systems. However, as the array is finite in the transverse direction, it acts like a partially transparent wall in an unusual interplay between Bloch waves and scattering theory: transmission and reflection coefficients, along with resonant phenomena for propagation through the wall, coexist with conduction along the quasi-one-dimensional (quasi-1D) array. Although the same coexistence exists for any real finite sample of periodic material, it is especially evident and exposed in the quasi-1D periodic array.

In order for quasi-1D guiding to exist, the individual scatterers making up the wall must be attractive. However, assuming elastic scattering, a freely propagating incident mode can be captured and guided along the array only if the array supports conducting states at $E>0$. It is easy to motivate the fact that an array of atoms (with each atom supporting an $E<0$ bound state) can give rise to an overall $E>0$ conducting state.

Consider a double-well potential, such that each individual well, when taken alone, admits a single bound state. At large separation, the wells will give rise to a degenerate doublet of symmetric and antisymmetric bound states. As the wells come closer together, the antisymmetric state rises in energy until it is pushed to $E>0$ and becomes a *p*-wave resonance, as described in Ref. [5], which is closely related to the concept of proximity resonances [6]. In Fig. 1, the bound-state energies for two and four scatterers are shown; as the scatterers come close together, the highest-energy bound state is pushed above threshold.

For the infinite wall, one way to understand the presence of $E>0$ guided states for the wall is to consider the limit where the scatterers are infinitely close together, thereby effectively forming a potential trough of some width w:

$$V(x,y)=\begin{cases}-V_0, & |x|<w,\\ 0, & |x|>w.\end{cases}$$

Since the above potential is separable, if the effective 1D well (about the $\hat{x}$ direction) admits an $E<0$ bound state, the trough admits a continuum of $E>0$ states which are bound along the $\hat{x}$ direction, because any wave number can be taken in the free $\hat{y}$ direction. Thus by analogy to other, more familiar systems, it seems reasonable that a wall of attractive scatterers could behave as a waveguide.

We further note that at low energies, a curved chain of discrete, attractive atoms approximates a continuous, curved waveguide, suggesting an efficient numerical method for modeling continuous waveguides via multiple-scattering methods. A related method is the boundary wall method in [7].

The remainder of this paper is divided into five parts. We begin, in Sec. II, with a brief review of Foldy's method of multiple scattering. In Sec. III, we apply Foldy's method to solve the Lippmann-Schwinger equation for a general periodic array of scatterers. In Sec. IV, we investigate diffraction and threshold resonances, uncovering a type of quasibound

*Electronic address: vaishnav@physics.harvard.edu

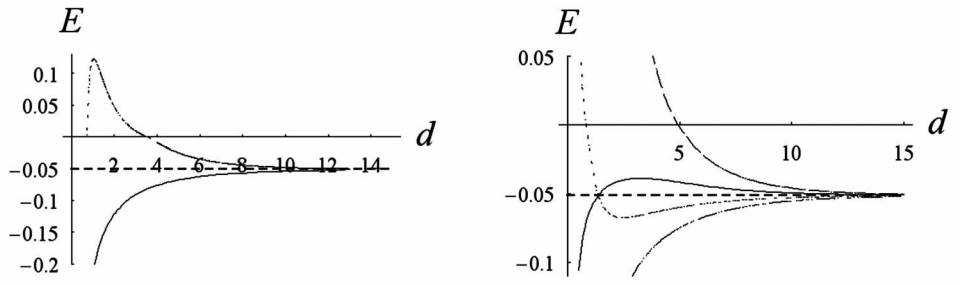

FIG. 1. Bound-state energies for two scatterers (left) and four scatterers (right) separated by distances d. The dashed line is the bound-state energy of an individual scatterer. For large d, the ground state is the completely symmetric eigenstate, while the highest-energy state is the completely antisymmetric eigenstate. As the scatterers come closer together, the antisymmetric eigenstate is pushed to positive energy. The scatterers are point scatterers modeling the s-wave scattering from a cylindrical well of depth $V_0=-0.8$ and radius $a=0.2$.

states which are related to guiding. In Sec. V we search for true guided states, and we calculate the band structure for a single infinite wall of attractive scatterers. We demonstrate that when individual scatterers have $E<0$ bound states, an array can support conducting states at positive energies $E>0$. Finally, in Sec. VI, we numerically demonstrate that if the array's symmetry is somehow broken, these conducting states can be used to guide a beam; i.e., the array can capture an incident wave focused on one end of the array, forcing it to propagate along the array and emerge on the other end.

II. BACKGROUND: FOLDY'S METHOD

The physical underpinning of all the resonance and interference phenomena which we discuss in this paper is multiple scattering, both within each unit cell and between different unit cells. To model multiple scattering, we make extensive use of Foldy's method [8], which we briefly review here. Consider a wave $\phi(\vec{r})$ incident on a collection of N identical point scatterers at positions $\{\vec{r}_1,\ldots,\vec{r}_N\}$, where $\vec{r}_n=(x_n,y_n)$. Applying the t-matrix formalism [9], we characterize a single scatterer at $\vec{r}_i$ by its t matrix,

$$t = s(k)|\vec{r}_i\rangle\langle\vec{r}_i|,$$

where $s(k)$ is a function of the wave number, $k=\sqrt{2mE}/\hbar$. The functional form of $s(k)$ is chosen to simulate the scatterer of interest under the constraint that $s(k)$ must satisfy the optical theorem

$$-\frac{2\hbar^2}{m}\,\mathrm{Im}\,s(k) = |s(k)|^2. \tag{1}$$

In the t-matrix formalism, the Lippmann-Schwinger equation for multiple scattering is

$$\psi(\vec{r}) = \phi(\vec{r}) + s(k)\sum_{i=1}^{N}\psi_i(\vec{r}_i)G_0(\vec{r},\vec{r}_i), \tag{2}$$

where

$$G_0(\vec{r},\vec{r}_0) = \frac{2m}{\hbar^2}\left[-\frac{i}{4}H_0^{(1)}(k|\vec{r}-\vec{r}_0|)\right] \tag{3}$$

is the 2D free-space retarded Green's function satisfying

$$(\vec{\nabla}^2+k^2)G_0(\vec{r},\vec{r}_0) = \frac{2m}{\hbar^2}\delta^{(2)}(\vec{r},\vec{r}_0)$$

and the various $\psi_i(\vec{r}_i)$ in Eq. (2) are defined recursively as

$$\psi_i(\vec{r}_i) = \phi(\vec{r}_i) + s(k)\sum_{\substack{j=1\\ j\neq i}}^{N}\psi_j(\vec{r}_j)G_0(\vec{r}_i,\vec{r}_j). \tag{4}$$

$\psi_i(\vec{r}_i)$ is the *effective* incoming wave function evaluated at the ith scatterer after scattering from each of the other scatterers, excluding the singular self-interaction of the ith scatterer. In the remainder of this paper, we set $\hbar=m=1$ and denote $s(k)$ as s.

Defining two $N\times 1$ column vectors $\vec{\phi}$ and $\vec{\psi}$, whose ith elements are given by $\vec{\phi}_i\equiv\phi(\vec{r}_i)$ and $\vec{\psi}_i\equiv\psi(\vec{r}_i)$, the Lippmann-Schwinger equation can be written as a simple matrix equation by inverting Eqs. (2)–(4) to yield

$$\vec{\psi} = \mathbf{M}^{-1}\vec{\phi}, \tag{5}$$

where

$$\mathbf{M} \equiv 1 - s\mathbf{G}$$

and the matrix $\mathbf{G}$ is defined by

$$G_{ij} \equiv \begin{cases} 0, & i=j, \\ G_0(\vec{r}_i,\vec{r}_j), & i\neq j. \end{cases} \tag{6}$$

$\mathbf{G}$ excludes the singular self-interactions of each scatterer with itself.

Substituting the values of $\vec{\psi}_i$ from Eq. (5) into Eq. (2) yields an expression for the scattered wave function:

$$\psi(\vec{r}) = \phi(\vec{r}) + s\sum_{i=1}^{N}G_0(\vec{r},\vec{r}_i)(\mathbf{M}^{-1}\vec{\phi})_i. \tag{7}$$

III. MULTIPLE SCATTERING FROM GENERAL PERIODIC STRUCTURES: CONNECTION TO BLOCH WAVES

The problem of guiding is related to finding conducting eigenstates for an array of scatterers. We discussed in Sec. I

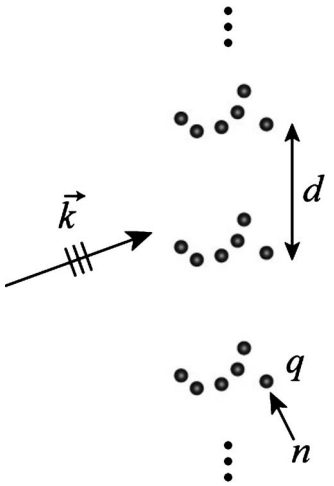

FIG. 2. Plane wave incident on array with Bravais vector $d\hat{y}$. The unit cell is indexed by q, and each individual scatterer is indexed by n.

how Bloch waves and scattering phenomena coexist in such systems. The usual 3D approach of reciprocal lattices could be adapted to 2D. We instead apply multiple-scattering theory, considering all of the multiple-scattering events within each unit cell as well as between different unit cells. The multiple-scattering approach, although more involved, yields detailed information about interference processes and also generalizes more easily to the introduction of disorder into the lattice.

In this section, we apply Foldy's method to solve the Lippmann-Schwinger equation for a plane-wave scattering from a general, infinite periodic array of clusters of point scatterers with a Bravais lattice spanned by $d\hat{y}$ (Fig. 2). The multiple-scattering solution in Eq. (5) would seem to require inversion of a bi-infinite matrix. In this section, however, we reduce the solution to inversion of an $N\times N$ matrix, where N is the number of scatterers per unit cell, and demonstrate how Bloch waves arise naturally from multiple-scattering theory. The resulting Lippmann-Schwinger equation resembles Eqs. (5) and (6) but with an effective scattering strength $\tilde{s}$ and an effective Green's matrix $\tilde{\mathbf{G}}$ which account for multiple scattering between unit cells.

Our approach turns out to be related to the Korringa-Kohn-Rostoker (KKR) method [10,11], with the variation that we have represented our scatterers by t matrices and have begun with an s-wave approximation. A related approach has been applied to study scattering from two-dimensional periodic slabs of scatterers embedded in three dimensions [12].

A. Multiple scattering from a periodic grating

Denote by $\vec{r}_n^{(q)}$ the position of the nth of N scatterers in unit cell q. Further suppose that all N scatterers in a unit cell are identical with t matrix given by s (the arguments in this section can easily be generalized to the case of nonidentical scatterers). Applying Foldy's method, we can write the Lippmann-Schwinger equation as

$$\psi(\vec{r}) = \phi(\vec{r}) + s\sum_{q=-\infty}^{\infty}\sum_{n=1}^{N} G_0(\vec{r},\vec{r}_n^{(q)})\psi_n^{(q)}(\vec{r}_n^{(q)}), \tag{8}$$

$$\psi_n^{(q)}(\vec{r}_n^{(q)}) = \phi(\vec{r}_n^{(q)}) + s\sum_{p=-\infty}^{\infty}\sum_{\substack{m=1\\(m,p)\neq(n,q)}}^{N} G_0(\vec{r}_m^{(p)},\vec{r}_n^{(q)})\psi_m^{(p)}(\vec{r}_m^{(p)}), \tag{9}$$

where $G_0(\vec{r}_m,\vec{r}_n)$ is the free-space Green's function ($\hbar=m=1$) from Eq. (3). Once again, if the effective incident wave-function amplitudes at the scatterers, $\psi_n^{(q)}(\vec{r}_n^{(q)})$ in Eq. (9), are known, the full wave function is determined using Eq. (8).

It is straightforward to recursively sum and reindex Eq. (9) to show that for an incident wave (normalized to unit flux along the $\hat{x}$ direction),

$$\phi(\vec{r}) = \frac{1}{\sqrt{k_x^{(0)}}}e^{i\vec{k}\cdot\vec{r}},$$

the solutions to Eq. (9) are reduced to finding the wave function amplitudes for a single unit cell, since

$$\psi_n^{(q)}(\vec{r}_n^{(q)}) = e^{ik_y qd}\psi_n^{(0)}(\vec{r}_n^{(0)}). \tag{10}$$

Let us focus on the N scatterers in the unit cell indexed by $q=0$. Using Eq. (10) on the right-hand side of Eq. (9), evaluated for $q=0$, we obtain

$$\psi_n^{(0)}(\vec{r}_n^{(0)}) = \phi(\vec{r}_n^{(0)}) + s\sum_{p=-\infty}^{\infty}\sum_{\substack{m=1\\(m,p)\neq(n,0)}}^{N} G_0(\vec{r}_m^{(p)},\vec{r}_n^{(0)}) \times e^{ik_y pd}\psi_m^{(0)}(\vec{r}_m^{(0)}). \tag{11}$$

We wish to separate off the $m=n$ term, which corresponds to multiple scattering between each scatterer and its periodic counterparts in other unit cells. It is in this term that we must exclude the self-interaction, which corresponds to $m=n$ and $p=0$. Breaking up the sum, we find

$$\begin{aligned}\psi_n^{(0)}(\vec{r}_n^{(0)}) &= \phi(\vec{r}_n^{(0)}) + s\sum_{\substack{p=-\infty\\p\neq 0}}^{\infty} G_0(k|p|d)e^{ik_y pd}\psi_n^{(0)}(\vec{r}_n^{(0)}) \\ &\quad + s\sum_{\substack{m=1\\m\neq n}}^{N}\left[\sum_{p=-\infty}^{\infty} G_0(\vec{r}_m^{(0)} + pd\hat{y},\vec{r}_n^{(0)})e^{ik_y pd}\right]\psi_m^{(0)}(\vec{r}_m^{(0)}) \\ &= \phi(\vec{r}_n^{(0)}) + sG_r\psi_n^{(0)}(\vec{r}_n^{(0)}) + s\sum_{m=1}^{N}\tilde{\mathbf{G}}_{mn}\psi_m^{(0)}(\vec{r}_m^{(0)}).\end{aligned} \tag{12}$$

In Eq. (12), G_r is a scalar quantity independent of the configuration of the unit cell and is given by

$$G_r \equiv s\sum_{p\neq 0} G_0(k|p|d)e^{ik_y pd} \tag{13}$$

and $\tilde{\mathbf{G}}$ is an $N\times N$ matrix defined as

$$\tilde{\mathbf{G}}_{mn} = \begin{cases} 0, & m = n, \\ G(\vec{r}_n^{(0)} - \vec{r}_m^{(0)}), & m \neq n, \end{cases} \tag{14}$$

where in Eq. (14) we used the lattice sum

$$G(\vec{r}) = \sum_{p=-\infty}^{\infty} G_0(\vec{r}, pd\hat{y}) e^{ik_y pd}. \tag{15}$$

A rapidly converging expression for $G(\vec{r})$ can be found in Eq. (A3) of Appendix A.

Defining vectors of wavelets

$$\vec{\phi}^{(0)} = \begin{pmatrix} \phi_1^{(0)}(\vec{r}_1^{(0)}) \\ \phi_2^{(0)}(\vec{r}_2^{(0)}) \\ \vdots \\ \phi_N^{(0)}(\vec{r}_N^{(0)}) \end{pmatrix},$$

$$\vec{\psi}^{(0)} = \begin{pmatrix} \psi_1^{(0)}(\vec{r}_1^{(0)}) \\ \psi_2^{(0)}(\vec{r}_2^{(0)}) \\ \vdots \\ \psi_N^{(0)}(\vec{r}_N^{(0)}) \end{pmatrix}, \tag{16}$$

we can solve for the wavelets in the $q=0$ unit cell:

$$\vec{\psi}^{(0)} = \frac{1}{1 - sG_r} \tilde{\mathbf{M}}^{-1} \vec{\phi}^{(0)}, \tag{17}$$

where we have defined

$$\tilde{\mathbf{M}} = \mathbf{I} - \tilde{s}\tilde{\mathbf{G}} \tag{18}$$

and

$$\tilde{s} = \frac{s}{1 - sG_r}. \tag{19}$$

The remaining wavelets in other unit cells are then simply determined by Eq. (10):

$$\vec{\psi}^{(q)} = e^{ik_y qd} \vec{\psi}^{(0)}. \tag{20}$$

The full wave function is finally given by substituting Eqs. (17) and (20) into Eq. (8):

$$\psi(\vec{r}) = \phi(\vec{r}) + \tilde{s} \sum_{p=-\infty}^{\infty} \sum_{n=1}^{N} G_0(\vec{r}, \vec{r}_n^{(p)}) e^{ik_y pd} (\tilde{\mathbf{M}}^{-1} \vec{\phi}^{(0)})_n \tag{21}$$

$$= \phi(\vec{r}) + \tilde{s} \sum_{n=1}^{N} (\tilde{\mathbf{M}}^{-1} \vec{\phi}^{(0)})_n \sum_{p=-\infty}^{\infty} G_0(\vec{r} - \vec{r}_n^{(0)}, pd\hat{y}) e^{ik_y pd} \tag{22}$$

$$= \phi(\vec{r}) + \tilde{s} \sum_{n=1}^{N} G(\vec{r} - \vec{r}_n^{(0)}) (\tilde{\mathbf{M}}^{-1} \vec{\phi}^{(0)})_n. \tag{23}$$

Note the similarity between Eqs. (23) and (7): one can go from a single unit cell to a repeating array simply by replacing the t matrix $s(k)$ with its renormalized version $\tilde{s}(\vec{k})$ and the free-space Green's function $G_0(\vec{r})$ with the effective Green's function $G(\vec{r})$. The wave function in Eq. (21) is a Bloch wave since

$$\psi(\vec{r} + d\hat{y}) = e^{ik_y d} \psi(\vec{r}).$$

We note that the renormalization and interference effects in a periodic grating are very similar to the effects encountered when a scatterer or a cluster of scatterers is placed in an external confining potential (see, e.g., [13,14]). The similarity arises because scattering in a confined geometry is also effectively a multiple-scattering problem: A particle can scatter once from the target, reflect from the confining potential, and scatter again. In the case of a cluster of scatterers confined to a hard-walled or periodic waveguide, the mapping to an array is in fact explicit; applying the method of images, the cluster becomes an infinite array where the effective "unit cells" are images of the confined cluster of scatterers.

IV. DIFFRACTION AND QUASIBOUND STATES

The result in Eq. (23) is in terms of superpositions of spherical waves. Alternatively, Eq. (23) could be written in a basis of plane and evanescent waves. Substituting Eq. (A3) into Eq. (23) yields a plane plus evanescent-wave expansion for the scattered wave:

$$\psi(\vec{r}) = \frac{e^{i\vec{k}_0 \cdot \vec{r}}}{\sqrt{k_x^{(0)}}} - \frac{i\tilde{s}}{d} \sum_{q=-\infty}^{\infty} \sum_{n=1}^{N} (\tilde{\mathbf{M}}^{-1} \vec{\phi}^{(0)})_n \frac{1}{k_x^{(q)}} e^{ik_x^{(q)} |x - x_n^{(0)}|} e^{ik_y^{(q)} (y - y_n^{(0)})}, \tag{24}$$

where the wave numbers of the diffracted beams are quantized by the Bragg condition:

$$k_y^{(q)} = k_y^{(0)} + \frac{2q\pi}{d}, \tag{25}$$

$$k_x^{(q)} = \sqrt{k^2 - (k_y^{(q)})^2}. \tag{26}$$

The values of q for which $k_x^{(q)}$ is real correspond to diffracted plane waves, while the remaining values of q correspond to evanescent waves. The set $\mathcal{Q}$ of open channels, corresponding to diffracted plane waves, is defined by $\mathcal{Q} = [\mathcal{Q}_{min}, \mathcal{Q}_{max}]$ where

$$\mathcal{Q}_{min} = \left\lceil -\frac{(k + k_y)d}{2\pi} \right\rceil, \tag{27}$$

$$\mathcal{Q}_{max} = \left\lfloor \frac{(k - k_y)d}{2\pi} \right\rfloor. \tag{28}$$

Equation (24) is in essence Bragg diffraction: the scattered wave consists of a finite number of diffracted plane waves propagating at the Bragg angles given by Eqs. (25) and (26) and an infinite number of evanescent waves.

In the far field, defined by $|x| \gg |x_n|$ for all n, only the diffracted beams survive, and the transmitted and reflected wave functions are

$$\psi_R(\vec{r}) = \sum_{q \in \mathcal{Q}} R_q \frac{1}{\sqrt{k_x^{(q)}}} e^{-ik_x^{(q)} x + ik_y^{(q)} y}, \tag{29}$$

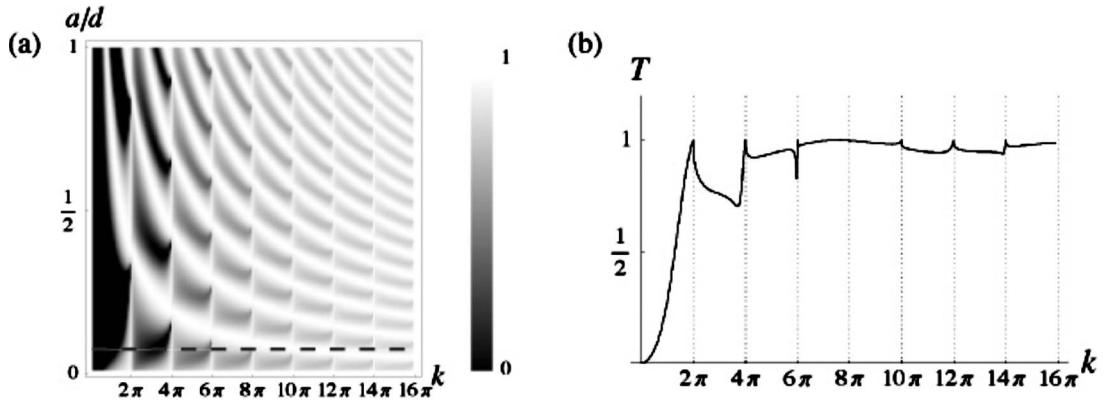

FIG. 3. (a) Transmission coefficient for scattering of an incident beam with wave number k from a wall of hard disks with radius a. The incident beam is at normal incidence ($k_y^{(0)}=0$). At low energies, the beam is fully reflected; at high energies the beam is almost entirely transmitted. Note the transmission resonances at $k=k_y^{(n)}$. (b) Structure of the resonances at $a=0.1$ [dashed line in (a)]. This figure also illustrates the breakdown of the s-wave approximation at high energies; classically, the limit of the transmission should not be exactly 1.

$$\psi_T(\vec{r}) = \sum_{q\in\mathcal{Q}} T_q \frac{1}{\sqrt{k_x^{(q)}}} e^{ik_x^{(q)}x + ik_y^{(q)}y}, \tag{30}$$

where the reflection and transmission coefficients R_q and T_q are given by [using Eq. (24)]

$$R_q = -\frac{i\tilde{s}}{d}\frac{1}{\sqrt{k_x^{(q)}}}\sum_{n=1}^{N}(\tilde{\mathbf{M}}^{-1}\vec{\phi}^{(0)})_n e^{ik_x^{(q)}|x_n^{(0)}|}e^{-ik_y^{(q)}y_n^{(0)}}, \tag{31}$$

$$T_q = \delta_q - \frac{i\tilde{s}}{d}\frac{1}{\sqrt{k_x^{(q)}}}\sum_{n=1}^{N}(\tilde{\mathbf{M}}^{-1}\vec{\phi}^{(0)})_n e^{-ik_x^{(q)}|x_n^{(0)}|}e^{-ik_y^{(q)}y_n^{(0)}}. \tag{32}$$

The quantities $|R_q|^2$ and $|T_q|^2$ correspond to the probability of reflection or transmission into the qth mode; the $q=0$ mode is the specular component. The total reflection and transmission probabilities for the wall of scatterers are given by

$$R = \sum_{q\in\mathcal{Q}} |R_q|^2, \tag{33}$$

$$T = \sum_{q\in\mathcal{Q}} |T_q|^2. \tag{34}$$

The value of the renormalized t matrix, $\tilde{s}$, is constrained by combining Eqs. (33) and (34) with the unitarity requirement $R+T=1$. This constraint is an analog of an optical theorem for the grating. The optical theorem for the single wall of scatterers is derived in Appendix B.

Threshold resonances and quasibound states

Since the signature of a bound or quasibound state is often a transmission resonance, we begin by examining the transmission coefficient of the array, Eq. (34). As illustrated in Fig. 3 for the single chain of atoms, resonances occur at energies such that $k_x^{(q)}\to 0$. Such resonances, called threshold resonances, correspond to energies at which one of the evanescent waves becomes a propagating diffracted beam. These threshold resonances are purely due to the periodicity of the array, and the resonance energies are independent of the type or configuration of the scatterers within an individual unit cell. Threshold resonances occur in atom-surface scattering as selective adsorption resonances [15], in x-ray diffraction as emergent beam resonances, and in acoustics as Parker resonances [16].

Near a threshold resonance—i.e., as $k\to k_y^{(q)}\pm\epsilon$—the lattice sum in Eq. (A7) yields

$$\lim_{k\to k_y^{(q)}\pm\epsilon} G_r = -\frac{i}{d}\frac{1}{\sqrt{\pm 2k_y^{(q)}\epsilon}}. \tag{35}$$

From Eqs. (19) and (35),

$$\lim_{k\to k_y^{(q)}\pm\epsilon} \tilde{s} = \frac{1}{G_r} = id\sqrt{\pm 2k_y^{(q)}\epsilon}. \tag{36}$$

From Eq. (36), the dependence of $\tilde{s}$ on the bare t matrix $s(k)$ cancels entirely near the threshold resonance. Exactly on threshold, $\tilde{s}=0$, which from Eqs. (31) and (32) yields $T=1$; the array becomes entirely transparent, and the incident beam is entirely transmitted (although with a phase). This transparency, which is a form of the Ramsauer-Townsend effect, is consistent with flux conservation, as the guided beam carries no flux away from the array.

Inserting Eq. (36) into Eq. (24), the scattered wave near threshold consists entirely of the emergent beam traveling along the $\hat{y}$ axis:

$$\lim_{k=k_y^{(q)}-\epsilon} \psi(\vec{r}) = e^{i\vec{k}\cdot\vec{r}} + \sum_{n=1}^{N}(\tilde{\mathbf{M}}^{-1}\vec{\phi}^{(0)})_n e^{-\sqrt{2k_y^{(q)}\epsilon}|x-x_n^{(0)}|}e^{ik_y^{(q)}(y-y_n^{(0)})} + O(\epsilon^{1/2}), \tag{37}$$

$$\lim_{k=k_y^{(q)}+\epsilon} \psi(\vec{r}) = e^{i\vec{k}\cdot\vec{r}} + \sum_{n=1}^{N}(\tilde{\mathbf{M}}^{-1}\vec{\phi}^{(0)})_n e^{i\sqrt{2k_y^{(q)}\epsilon}|x-x_n^{(0)}|}e^{ik_y^{(q)}(y-y_n^{(0)})} + O(\epsilon^{1/2}). \tag{38}$$

Figure 4 illustrates the probability density above [Fig. 4(b)]

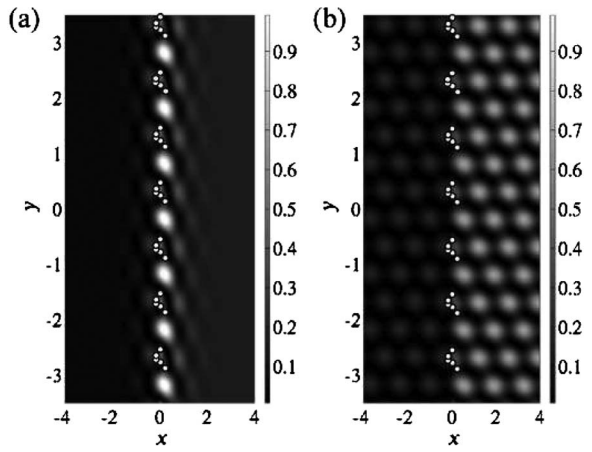

FIG. 4. Threshold resonance for a unit cell with five randomly placed scatterers (hard disks with $a=0.1$) depicted by the dots in the figure). The full wave function just above and below threshold is given by Eqs. (37) and (38). For clarity, we plot only the scattered wave function; the incident wave is a plane wave and would be added to the scattered wave function to obtain the full wave function. (a) The quasibound state just below resonance, at wave number $kd=2\pi-0.3$, becomes unbound (b) just above resonance, at $kd=2\pi+0.3$.

and below [Fig. 4(a)] a threshold resonance for a wall of hard disks. For clarity, the incident wave function $e^{i\vec{k}\cdot\vec{r}}$ is omitted from $\psi(\vec{r})$ in Eqs. (37) and (38) when plotting $|\psi(\vec{r})|^2$ in Fig. 4. Approaching the threshold from below, the evanescent beam, which is about to emerge, dominates the scattering. The scattered state consists almost entirely of a state which is evanescent along the $\hat{x}$ direction [Fig. 4(a)] but becomes progressively more weakly bound as we approach threshold. At threshold, the scattered state merges with the continuum, and for wave numbers just above threshold, the scattered state is weakly unbound in the $\hat{x}$ direction [Fig. 4(b)]. The threshold resonance thus corresponds to quasibound states which conduct along the wire. Although these quasibound states constitute, in some sense, a form of guiding, they are not truly conducting states. The $O(\epsilon^{1/2})$ term in Eqs. (37) and (38) is due to coupling to other unbound states. The $\psi(\vec{r})$ states in Eqs. (37) and (38) are thus quasibound rather than being truly bound, and they have finite lifetimes. Similar states, known as Rayleigh-Bloch waves, exist in many other physical systems ranging from ocean coastlines [17] to acoustics [16].

V. CONDUCTING STATES

Motivated by the presence of quasibound states, we now refine our search to find genuine conducting eigenstates. An array of attractive scatterers, in the limit where the scatterers are closely spaced, should resemble a quasi-1D potential trough embedded in 2D and give rise to a set of states which are purely bound along the array. Such conducting states would be evanescent in the $\hat{x}$ direction but free in the $\hat{y}$ direction and thus correspond to states with wave vectors

$$\vec{k} = i\kappa_x\hat{x} + k_y\hat{y}. \tag{39}$$

In contrast to the quasibound states in Sec. IV, the truly conducting states would contain *only* such wave vectors; in a time-dependent sense, a wave packet injected into such a state would conduct forever. Unlike the quasibound states, bound states depend strongly on the properties of the grating and do not necessarily exist for an arbitrary periodic grating. For example, a periodic array of repulsive scatterers, while possessing infinitely many quasibound states, would not have any truly conducting states.

For a single point scatterer in free space, two criteria characterize a bound state: the state is (i) localized (has negative energy) and (ii) is a pole of the t matrix (the interpretation of this criterion is that the bound state is a scattering state which exists even in the absence of an incoming wave function). For an array of scatterers, Foldy's method transforms the Lippmann-Schwinger equation into the matrix equation (17), which can be rewritten as

$$[(1 - sG_r)\tilde{\mathbf{M}}]^{-1}\vec{\psi}^{(0)} = \vec{\phi}^{(0)}. \tag{40}$$

The existence of a scattered wave function for a zero incoming wave function implies the existence of a homogeneous solution to Eq. (40). States which exist in the absence of an incoming wave must exist at values of $\vec{k}$ which are roots of the secular equation

$$(1 - sG_r)^N \det \tilde{\mathbf{M}} = 0. \tag{41}$$

This secular equation is strongly dependent on the configuration of the unit cell and must be solved for a particular grating. We shall here focus on the single wall of atoms, which is the most common experimental setup [2–4]. For the single wall, $\tilde{\mathbf{M}}=\mathbf{I}$, and Eq. (41) simplifies to

$$1 - sG_r = 0, \tag{42}$$

implying, from Eq. (19), that a bound state corresponds to a pole of the renormalized t matrix, $\tilde{s}$.

In order to find conducting states, we evaluate $\tilde{s}$ on a grid of values of (κ_x, k_y) and numerically search for poles of the form given in Eq. (39) with corresponding energy

$$E = \frac{1}{2}\sqrt{-\kappa_x^2 + k_y^2}.$$

Bound states with $E>0$ correspond to those poles of the renormalized t matrix for which $|k_y|>|\kappa_x|$. We used the t matrix in Eq. (C3) to simulate an infinite wall of attractive cylindrical wells with depth $V_0=-8.0$ and radius $a=0.2$, so that an individual well allowed a single bound state just barely below threshold (at $E=-0.05$, or $\kappa=-\sqrt{2E}=0.32i$). Figure 1 depicts how arrays of two or four such wells support bound states above $E=0$ as the wells are placed close together. Figures 5(a), 5(c), and 5(e) show the manifold of poles in $\vec{k}$ space for an infinite wall of scatterers for three different lattice constants. In each figure, the solid curves correspond to the manifolds of conducting states for the array and the dashed curves correspond to the bound-state energies of a single scatterer, given by

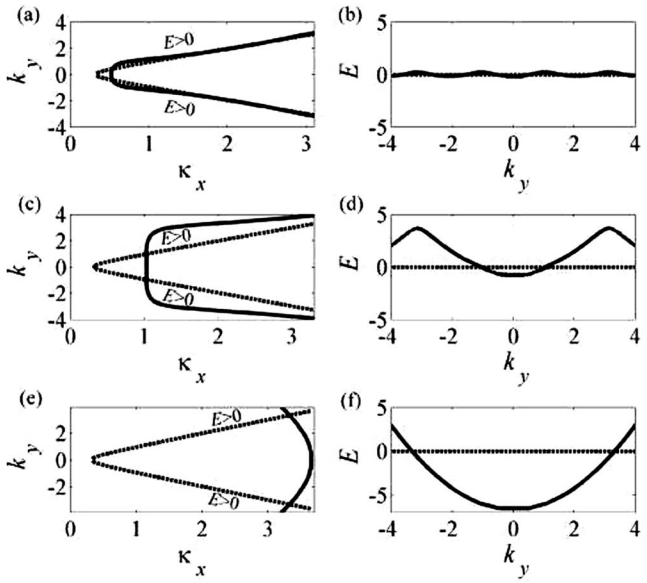

FIG. 5. (a),(c),(e) show the curves along which $\tilde{s}(i\kappa_x,k_y)$ has poles (the symmetry across $k_y=0$ is due to reflection symmetry of the array along $y=0$). These curves correspond to manifolds of conducting states bound in the x direction and propagating along the array. The dashed curves, for comparison, are contours of wave vectors corresponding to the bound-state energy of a single scatterer. (b),(d), (f) show the band structure (E vs k_y) for the conducting states. (a),(b) correspond to a lattice constant $d=3.0$; (c),(d) to $d=1.0$; and (e),(f) to $d=0.202$. As the wells approach each other, the bands are increasingly perturbed from the single-scatterer limit. In all cases, conducting states are present at $E>0$.

$$-\kappa_x^2 + k_y^2 = -\kappa^2.$$

A more traditional view of the band structure for each potential is presented in Figs. 5(b), 5(d), and 5(f), where the energies of the conducting states versus k_y have been plotted. Figures 5(a) and 5(b) correspond to a large well separation ($d=3.0$), Figs. 5(c) and 5(d) to an intermediate well separation ($d=1.0$), and Figs. 5(e) and 5(f) to a small well separation ($d=0.202$). When the wells are far apart, the collective bound-state is near the bound state energy of a single scatterer, but as the wells approach each other, bound states occurring at $E>0$ start to appear. These states are particularly interesting since they could, in principle, be accessed by a propagating incident wave. As a demonstration, Fig. 6 illustrates that an incident propagating plane wave can couple into a state which is bound along the waveguide. Note that the periodicity of the guided portion of the wave is not the periodicity of the lattice.

VI. ARRAYS OF ATOMS AS WAVEGUIDES

We now apply the arguments of the previous sections to demonstrate that a wall of atoms might be used to guide waves. By guiding, we mean that if an incident beam is focused on some part of the grating, the scattered wave propagates along the grating for a long distance. In Secs. IV and V, we discussed the existence of states that are either

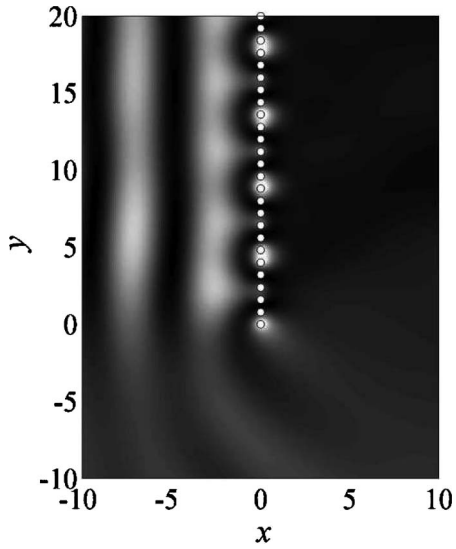

FIG. 6. Plane waves at normal incidence ($k=0.7$) scattering into a conducting state; scatterers (depicted by dots in the figure) are soft disks with $V_0=-8.0$, $a=0.2$, and $d=0.8$ (the same scatterers as in Figs. 1 and 5). This figure is a numerical demonstration that a propagating incident wave can couple into an $E>0$ conducting state of the array if the translational invariance of the array is broken. Coupling into the conducting state with a plane wave does not constitute guiding, as the incident wave already has amplitude everywhere.

quasibound or bound along the infinite array. These states, as such, are not an example of transport; being translationally invariant along the array, they can only be accessed by initial conditions that are already translationally invariant, such as plane waves. Transport along the array requires that the array have a symmetry breaking point where an incident wave can be injected. In particular, in order for a localized beam aimed at the array to conduct, the array must have a defect or an end. The asymmetry will of course affect the properties of the grating—e.g., diffraction, impedance, etc. While we can use our results on the infinite array as a basis for studies of guiding in related systems, the infinite array itself is not a waveguide.

A. Guiding by a semi-infinite array

Consider an incident beam

$$\phi(\vec{r}) = \frac{1}{2\pi}\int_{-\pi/2+\beta}^{\pi/2+\beta} g(\theta_k-\beta)e^{i\vec{k}(\theta_k)\cdot\vec{r}}d\theta_k, \tag{43}$$

where $g(\theta_k)=e^{-(\theta_k/w)^2}$. Equation (43) represents a beam incident from the right, focused on the scatterer at $\vec{r}=0$ and rotated by an angle β from the positive x axis. An incident beam [Eq. (43) with $\beta=0$ (normal incidence)] is shown in Fig. 7(a). As $w\to 0$, $\phi(\vec{r})$ approaches a plane wave, and for $w\to\infty$, $\phi(\vec{r})$ becomes a spherical wave with its form related to the Fourier transform of the spherical wave $J_0(kr)$. In the following, we are interested in intermediate values of w, for which Eq. (43) represents a focused beam.

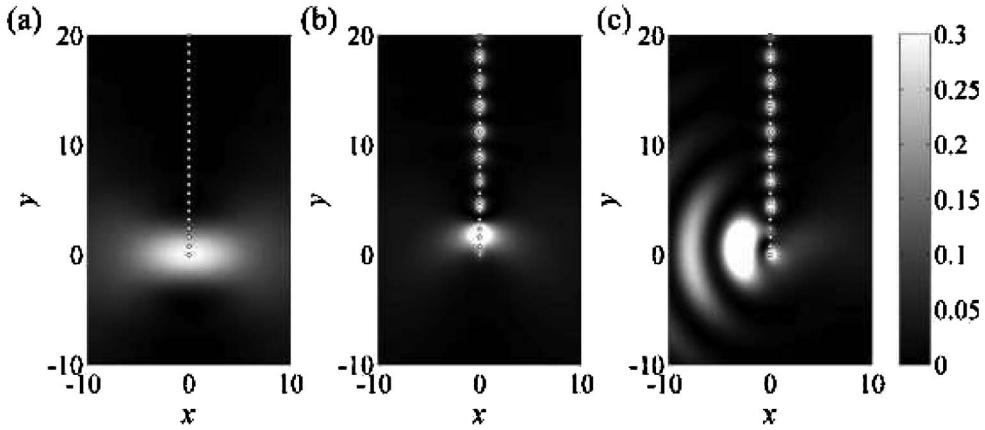

FIG. 7. Guiding of a focused beam with $k=0.7$. The scatterers are indicated by dots. These plots show the probability densities of (a) the incident beam, focused on the end of the array. (b) The scattered wave, which is guided along the array, and (c) the full scattered wave function (incident plus scattered). The individual scatterers are attractive wells with the same form and lattice constant as in Figs. 5(e) and 5(f).

Using our results for the infinite array as a guide, we take a purely numerical approach to the study of guiding in finite and semiinfinite arrays, as these systems are difficult to treat analytically. Analytical studies (e.g., Refs. [18,19]) typically conclude that scattering from a semiinfinite array reproduces certain major features of an infinite array: resonances, diffraction, etc. The main difference is that in the semi-infinite case, a spherical wave emanates from the end of the array. Most studies of semi-infinite arrays begin with the infinite solution and derive this spherical edge wave as a correction term.

We demonstrate guiding numerically in Fig. 7. The scatterers are closely spaced, and the focused beam is aimed at the end of the array. In Fig. 7(c), a guided state clearly propagates along the array. The guiding occurs at low energies, near bound states of the infinite array. Guiding does not occur for repulsive scatterers, confirming that the coupling is to the true bound states of the array rather than the quasibound states.

The guiding is robust and extends to gently curved and finite walls as demonstrated in Fig. 8, where a beam focused on one end of a curved wall emerges at the other end. The scatterers are effectively behaving like a light pipe for a matter wave. If the wall is curved sharply relative to the wavelength of the incident beam, amplitude leaks out as adiabaticity breaks down.

In this section, we have demonstrated via numerical simulations that the $E>0$ conducting states of the array can be exploited to guide waves along a semi-infinite wall of attractive, closely spaced scatterers. The physical explanation is that a semi-infinite wall of attractive potentials behaves like a trough and furthermore that, because the trough has an end, it is possible to couple into conducting states via injecting a beam into the end.

B. Effective cross section for conduction along the wire

From Figs. 7 and 8, it appears that an incident beam of particles focused on one end of a wall of scatterers can be efficiently guided to the other end. In this section, we provide a quantitative estimate of this guiding efficiency. Consider a focused beam $\phi(\vec{r})$ [Eq. (43)] of energy $E=\frac{1}{2}k^2$ with normal incidence ($\beta=0$) to the wall of scatterers. Such an initial incident beam has nonzero flux j_{inc} along the x direction, where

$$j_{inc}=\int_0^{\pi} d\theta[k\cos(\theta)]\exp[-2(\theta/w)^2].$$

The scattered flux can be calculated by evaluating the flux of the scattered wave function $\psi_s(\vec{r})$ over any contour which completely surrounds the scatterers. Finally, the total cross section can be simply evaluated by integrating the scattered flux over the desired contour and dividing by j_{inc}. For the wall of scatterers, the total cross section σ can be calculated over the contour shown in Fig. 9, giving

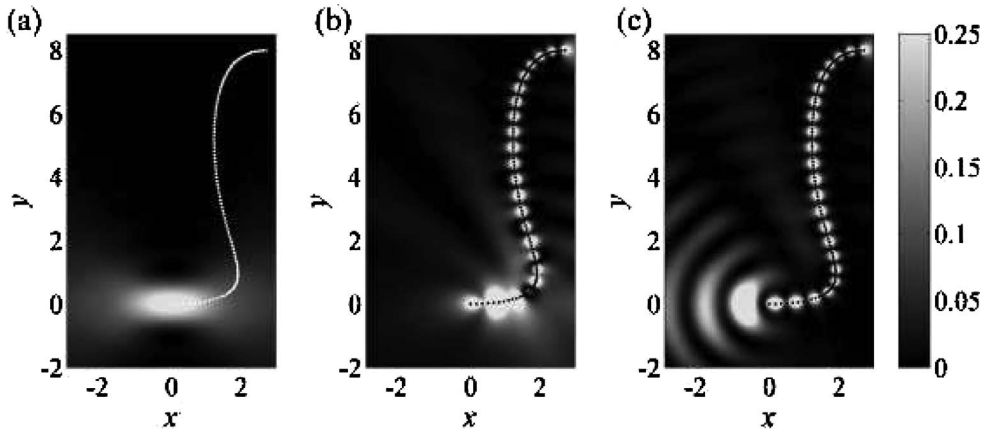

FIG. 8. Guiding of a focused beam along a finite wall; $k=3\pi$. The scatterers (depicted by dots in the figure) are attractive disks with $V_0=-10$, $a=0.2$. These plots show the probability densities of (a) the incident beam, (b) the scattered wave, and (c) the full scattered wave function (incident plus scattered). In (b), amplitude visibly leaks away near the sharp bend near $y=0$, as a consequence of nonadiabaticity.

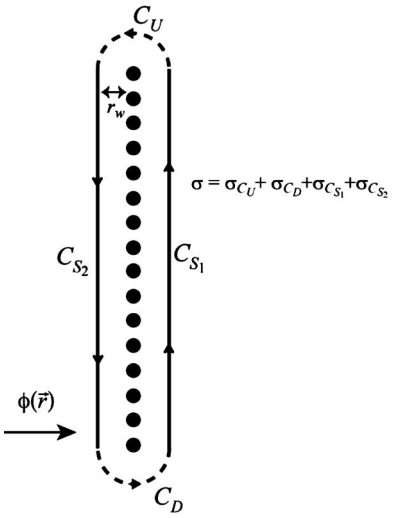

FIG. 9. The "stadium"-like contour used to evaluate the total cross section σ for the wall of scatterers. The shortest distance from any point on the contour to the wall is r_w. For an incident beam focused on the bottom of the wall of scatterers (indicated by the arrow), the fraction of particles "transported" along the wall is given roughly by σ_{C_U}/σ.

$$\sigma = \frac{1}{j_{inc}} \int_C d\vec{a}\, \mathrm{Im}[\psi_s^*(\vec{a}) \vec{\nabla} \psi_s(\vec{a})] = \sigma_{C_U} + \sigma_{C_D} + \sigma_{C_{S_1}} + \sigma_{C_{S_2}}, \tag{44}$$

where $\sigma_{C_{U(D)}}$ is the contribution to the total cross section from particles scattered through the upper (lower) semicircles.

As long as the contour encloses all the scatterers, the value of σ is independent of the choice of contour. However, $\sigma_{C_{U(D)}}$ and $\sigma_{C_{S_{1(2)}}}$ will depend on the value of r_w for the contour shown in Fig. 9. We are interested in estimating the fraction of scattered particles transported along the wire for an incident beam which is focused on the bottom of the wall of scatterers; i.e., we are interested in the ratio of σ_{C_U}/σ (assuming each incident particle is scattered). We should therefore choose r_w such that $r_w/L \ll 1$, where $L=Nd$ is the length of the wall of N scatterers with spacing

Figure 10(a) gives σ (in units of $10^4 d$) as a function of $kd=\sqrt{2E}$ for a system of $N=150$ square well scatterers characterized by $V_0=-8$, $d=0.8$, and $a=0.2$ [in addition, $w=1$ was chosen for $\phi(\vec{r})$ in Eq. (43)]. As can be seen from Fig. 10(a), σ increases with decreasing kd, although for the range of kd plotted in Fig. 10(a), σ is still much larger than the spatial spread of the incident wave function so that essentially all of the incident particles are scattered. In order to estimate the amount of transport along the scatterer wall, the ratio of the scattered flux through the other end of the wall is taken with the total scattered flux, which is simply equal to σ_{C_U}/σ; this ratio is shown in Fig. 10(b). Here, the fraction of scattered particles which are transported along the wire can reach up to 30% and oscillate with k. Note that the oscillations are related to the actual length of the wall; if the number of scatterers (and hence the array's length) is doubled, the period of the oscillations would roughly be doubled too. For $0.38\pi \leqslant k \leqslant 0.53\pi$, σ_{C_U}/σ oscillates slightly about $\sigma_{C_U}/\sigma \approx 12\%$. This means that even for a beam of particles with a distribution of incident energies (possibly due to thermal effects), at least 12% of the incident particles will still be transported along the wire. Also note that in these calculations, $r_w=10d$ so that $r_w/L=1/40 \ll 1$. It is interesting to observe that for a beam incident only on the lowermost scatterer and for the case of isotropic scattering (i.e., neglecting multiple scattering), the amount of scattered particles transported through the same region relative to the total scattered flux would be given by $2r_0/(2\pi L) \approx 0.8\%$. Thus the wall of scatterers can enhance the scattering along a given direction by a factor of almost 40.

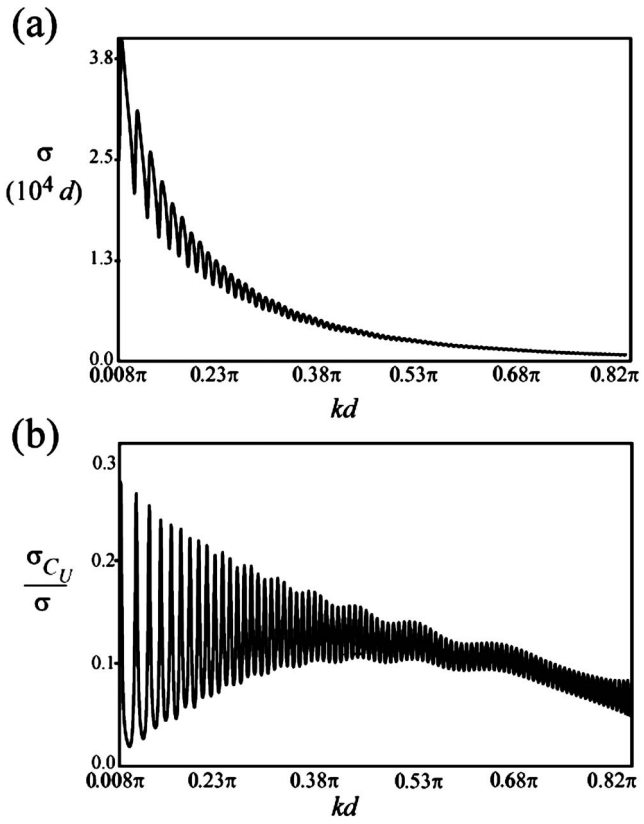

FIG. 10. (a) The total cross section σ in units of $10^4 d$ (where d is the lattice spacing) for $N=150$ square well scatterers ($V_0=-8$, $a=0.2$, $d=0.8$) as a function of kd. The incident beam is focused upon the bottom scatterer, with $w=1$. Since σ is much greater than the spread of the incident beam, it can be safely assumed that each incident particle is scattered. Therefore in order to obtain the number of particles which are transported along the scatterer wall, one must simply calculate σ_{C_U}/σ, shown in (b). As can be seen, up to 30% of all scattered particles can be transported along the wire (compared with only 0.8% if the scattering was assumed to be isotropic).

VII. CONCLUSIONS AND FUTURE DIRECTIONS

In this paper, we have examined scattering from and guiding by quasi-1D periodic gratings of scatterers embedded in

2D. This system is a good laboratory for highlighting the coexistence of scattering phenomena, such as transmission, reflection, and resonance, with features typical of periodic systems, such as band structure, diffraction, and conduction along the array. Arranging individual atoms on substrates, often in patterns far more intricate than gratings, has become an established experimental technique [2–4,20]. The motivation for our study is thus that atomic arrays can be built, have been successfully modeled by multiple scattering theories, [21–23], and can potentially serve as a waveguide for other particles.

In order to investigate the use of atomic arrays for guiding, we have developed a multiple-scattering theory (related to the KKR method) for quasi-1D gratings of *s* wave scatterers, embedded in 2D. The central physics is related to Bloch's theorem; we can obtain the full scattered wave function from the solution for a single unit cell by replacing the *t* matrix of an individual scatterer with its renormalized version and the free-space Green's function with an effective Green's function. We have used this result to discuss and to examine some general features of scattering from a single chain of atoms, such as resonances, quasibound states, and conducting states. Finally, we have demonstrated numerically that conducting states of the semiinfinite or finite array can be used to guide waves along straight or curved walls with up to 30% guiding efficiency.

The properties of the scattering and guiding studied here have strong analogs in optical systems, such as planar waveguides, optical fibers, and glass tabletops. For the latter, light incident on a sheet of glass at an angle and far from any edge is partially reflected and transmitted directly. Some of the light is transmitted and reflected indirectly, propagating inside the waveguide with attenuation by incomplete internal reflection. On the other hand, light incident on a (symmetry breaking) edge can be partially reflected, but mostly enters the sheet of glass and is trapped inside by total internal reflection. Due to its resonant modes, our system has shown analogs to each of these optical phenomena and others.

This work can be extended in a number of directions. We have chosen to embed our system in 2D because 2D is the relevant dimensionality for electrons in surface states scattering from atoms adsorbed on a metallic surface. With a change in the free-space Green's function, one could, however, revise the entire theory to treat a quasi-1D array embedded in 3D, such as might be relevant if the scatterers were atoms confined to an optical lattice. The physics of renormalization and interference in a 3D system would be very similar, and presumably identical guiding effects would arise.

Among the reasons that we have taken a multiple-scattering approach to the system is that it can be generalized to the introduction of impurities or defects into the array. We have discussed how symmetry breaking is required for guiding to occur. Introducing an impurity or defect into an infinite array is one way of breaking symmetry, with the impurity behaving as an antenna capable of drawing the incident wave into the conducting state. The problem of impurities in the array is also interesting in the sense that the array with an impurity becomes a scattering system in the conducting mode, yielding, in essence, a scattering theory within a scattering theory. The question of guiding in a system with disorder may also be of interest from the perspective of Anderson localization. Interesting questions arise as to how to maximize the guiding efficiency, for example, by impedance matching the array's end to free space. Finally, Foldy's method has recently been extended to include Rashba spin-orbit coupling [24], and it may be possible to modify the results of this paper to examine spintronic versions of guiding.

ACKNOWLEDGMENT

E.J.H. and M.A. acknowledge support from the National Science Foundation under NSF Grant No. CHE-0073544.

APPENDIX A: RELEVANT LATTICE SUMS

Equations (13) and (15) are in the form of spherical waves. We would like to find a more useful expression for Eq. (15) and also a more rapidly convergent expression for Eq. (13). Sums involving Hankel functions converge to the plane-wave limit very slowly. The physical implication of this slow convergence is that edge effects are more important than one might expect; many scatterers are required to build an "infinite" wall.

1. Plane-wave form of effective Green's function

The Green's function for an infinite array of scatterers, as expressed in spherical waves, is

$$G(\vec{r}) = \sum_{n=-\infty}^{\infty} G_0(\vec{r},\vec{r}_n)e^{ik_y nd}. \tag{A1}$$

Substituting the two-dimensional free-space Green's function [Eq. (3)], we find that

$$\begin{aligned} G(\vec{r}) &= -\frac{i}{2}\sum_{n=-\infty}^{\infty} H_0^{(1)}(k|\vec{r}-\vec{r}_n|)e^{ik_y nd} \\ &= -\frac{i}{2\pi}\int_{-\infty}^{\infty}\frac{dk_y'}{k_x'}e^{i(k_x',k_y')(x,y)}\sum_{n=-\infty}^{\infty}[e^{-i(k_y'-k_y)d}]^n, \end{aligned} \tag{A2}$$

where we have used the integral form of the Hankel function in the right half plane ($x>0$). Using

$$\sum_{n=-\infty}^{\infty}[e^{i(k_y'-k_y)d}]^n = \frac{2\pi}{d}\sum_{n=-\infty}^{\infty}\delta\left(k_y'-k_y+\frac{2n\pi}{d}\right),$$

we can do the integration, yielding the sum of plane waves at real and imaginary Bragg angles,

$$\begin{aligned} G(\vec{r}) &= -\frac{i}{d}\sum_{n=-\infty}^{\infty}\frac{1}{k_x^{(n)}}e^{ik_x^{(n)}|x|}e^{ik_y^{(n)}y} \\ &= -\frac{i}{d}e^{ik_y y}\sum_{n=-\infty}^{\infty}\frac{1}{k_x^{(n)}}e^{ik_x^{(n)}|x|}e^{(-2in\pi/d)y}, \end{aligned} \tag{A3}$$

where we have taken the absolute value to ensure convergence and

$$k_y^{(n)} \equiv k_y - \frac{2n\pi}{d},$$

$$k_x^{(n)} = \sqrt{k^2 - (k_y^{(n)})^2}$$

define wave vectors oriented at the Bragg angles. Imaginary values of $k_x^{(n)}$ correspond to evanescent modes and are present only in the near field.

This idea connects to the phenomenon of a "healing length" when examining reflections from a corrugated wall. We note that $G(\vec{r})$ is singular as we approach the origin; while the singularity is not evident in Eq. (A3), it is readily apparent in Eq. (A2). Reindexing, we find

$$G(\vec{r}) = -\frac{i}{k_x d} e^{ik_x|x|} e^{ik_y y} - \frac{i}{d} e^{ik_y y} \sum_{n=1}^{\infty} \left(\frac{1}{k_x^{(-n)}} e^{ik_x^{(-n)}|x|} e^{(2in\pi/d)y} + \frac{1}{k_x^{(n)}} e^{ik_x^{(n)}|x|} e^{-(2in\pi/d)y} \right). \tag{A4}$$

The wave function is a Bloch wave:

$$\psi(\vec{r} + d\hat{y}) = e^{ik_y d} \psi(\vec{r}),$$

with $E = \frac{1}{2}k^2 = \frac{1}{2}\sqrt{(k_x^{(n)})^2 + (k_y^{(n)})^2}$.

2. Kummer's method: Extracting the singularity

As in Refs. [13] and [25], we want to apply Kummer's method to extract the singularity from Eq. (A3) and also to obtain a rapidly convergent expression for the renormalized scattering strength $\tilde{s}$ [Eq. (13)]. We begin rewriting Eq. (13) as

$$G_r = \lim_{\vec{r}\to\vec{0}} [G(\vec{r}) - G_0(\vec{r})] = \lim_{\vec{r}\to\vec{0}} \{[G(\vec{r}) - S(\vec{r})] + [S(\vec{r}) - G_0(\vec{r})]\}, \tag{A5}$$

where $S(\vec{r})$ is a sum chosen to cancel the log singularity of the Hankel function. Looking at Eq. (A3), we choose the following form for $S(\vec{r})$:

$$S(\vec{r}) = -\frac{1}{\pi} \sum_{n=1}^{\infty} \frac{1}{n} e^{(2n\pi/d)|x|} \cos\left(\frac{2n\pi y}{d}\right).$$

With this choice of $S(\vec{r})$, we are extracting the zero-energy limit from the singular sum in Eq. (A4), evaluated (for simplicity) for a normally incident wave. The choice of $S(\vec{r})$ is not unique; our motivation for choosing this particular form of $S(\vec{r})$ is that we know that it will contain the logarithmic singularity. From Eq. (A1) we see that the zero-energy limit of the Green's function corresponds to the limit of a Hankel function as we approach the origin, and thus the zero-energy limit of the sum will be singular.

We shall proceed to show that although both $S(\vec{r})$ and $G(\vec{r})$ separately diverge logarithmically at the origin,

$$\lim_{\vec{r}\to\vec{0}} [S(\vec{r}) - G_0(\vec{r})]$$

is finite. We first find a closed form of $S(\vec{r})$:

$$S(\vec{r}) = -\frac{1}{\pi} \mathrm{Re} \sum_{n=1}^{\infty} \frac{1}{n} (e^{(2\pi/d)|x|} e^{2i\pi y/d})^n.$$

We can now use

$$\mathrm{Re} \sum_{n=1}^{\infty} \frac{Z^n}{n} = -\frac{1}{2} \ln |1 - Z|^2$$

to rewrite

$$S(\vec{r}) = \frac{1}{2\pi} \ln[e^{(2\pi/d)|x|}(e^{(-2\pi/d)|x|} - e^{(\pi/d)|x|} e^{2i\pi y/d}) \times (e^{(-2\pi/d)|x|} - e^{(\pi/d)|x|} e^{-2i\pi y/d})] = \frac{1}{2\pi} \ln\left\{ 2e^{(2\pi/d)|x|} \left[\cosh\left(\frac{2\pi}{d}x\right) - \cos\left(\frac{2\pi}{d}y\right) \right] \right\}.$$

Using this form, it is simple to take the limit

$$\lim_{\vec{r}\to\vec{0}} S(\vec{r}) = -\frac{1}{\pi} \ln\left(\frac{kd}{2\pi}\right) + \frac{1}{\pi} \ln kr. \tag{A6}$$

Subtracting the limiting form of the Hankel function,

$$\lim_{\vec{r}\to\vec{0}} G_0(kr) = -\frac{i}{2} + \frac{\gamma - \ln 2}{\pi} + \frac{1}{\pi} \ln kr,$$

from Eq. (A6), we find

$$\lim_{\vec{r}\to\vec{0}} [S(\vec{r}) - G_0(\vec{r})] = -\frac{1}{\pi} \ln\left(\frac{kd}{4\pi}\right) + \frac{i}{2} - \frac{\gamma}{\pi},$$

which is finite. Returning to Eq. (A5), we find that another form of $G(\vec{r})$ is

$$G(\vec{r}) = -\frac{i}{d}\frac{1}{k_x} e^{ik_x|x|} - \frac{i}{d} \sum_{n=1}^{\infty} \left[\frac{1}{k_x^{(-n)}} e^{ik_x^{(-n)}|x|} e^{i(k_y + 2in\pi/d)y} + \frac{1}{k_x^{(n)}} e^{ik_x^{(n)}|x|} e^{i(k_y - 2in\pi/d)y} - \frac{d}{in\pi} e^{(2n\pi/d)|x|} \cos\left(\frac{2n\pi y}{d}\right) \right] - \frac{1}{\pi} \ln\left(\frac{kd}{4\pi}\right) + \frac{i}{2} - \frac{\gamma}{\pi},$$

and from this expression, we can calculate G_r:

$$G_r = \lim_{\vec{r}\to\vec{r}_0} [G(\vec{r}) - G_0(\vec{r})] = \frac{-i}{k_x d} - \frac{i}{d} \sum_{n\neq 0} \left(\frac{1}{k_x^{(n)}} - \frac{d}{2i|n|\pi} \right) - \frac{1}{\pi} \ln\left(\frac{kd}{4\pi}\right) + \frac{i}{2} - \frac{\gamma}{\pi}. \tag{A7}$$

In the special case where the incident plane wave is normal to the array, this expression is identical to G_r for a scatterer at any location in a periodic wire. In the general case, the value of G_r differs in the values of $k_x^{(n)}$, which now depend on the incoming wave function.

APPENDIX B: UNITARITY AND THE SINGLE WALL

Simplifying Eqs. (31) and (32) to the case of a single chain of atoms, the reflection and transmission probabilities are

$$R_q = -\frac{i\tilde{s}}{d}\frac{1}{\sqrt{k_x^{(0)}k_x^{(q)}}},$$

$$T_q = \delta_{q0} + R_q. \tag{B1}$$

The unitarity requirement $T+R=1$ can be shown to yield the following constraint on $\tilde{s}$, which resembles the ordinary optical theorem, Eq. (1):

$$-\operatorname{Im}\tilde{s} = |\tilde{s}|^2 \sum_{q\in\mathcal{Q}} \frac{1}{k_x^{(q)}d}. \tag{B2}$$

Using Eqs. (19) and (A7), it is straightforward to verify that $\tilde{s}$ satisfies the unitarity condition, Eq. (B2), as long as the single-scatterer t matrix $s(k)$ satisfies the free-space unitarity condition, Eq. (1). In the limit $kd\to 0$, our results approach those for a continuous wall of scatterers. An alternate method for treating a continuous wall is the boundary wall method [7] where the wall is discretized into a set of pseudoscatterers. The boundary wall method has been shown to be equivalent to building a wall out of point scatterers-with the exception that the self-interaction, which was omitted in Eq. (4), has been left in the calculation, rendering the individual pseudoscatterer unphysical since its t matrix no longer satisfies the optical theorem in Eq. (1). Our formalism, though significantly more complicated, has the advantage of corresponding physically to building a wall out of individual atoms.

APPENDIX C: SIMULATING POTENTIALS WITH A t MATRIX

1. Hard disk

The 2D hard disk is simulated by requiring that the wave function go to zero at a radius a from the scatterer. It is shown (see, e.g., [26]) that this corresponds to a t matrix

$$s(k) = -2i\frac{J_0(ka)}{H_0^{(1)}(ka)}.$$

2. Soft disk

Another example of a potential for which we can analytically calculate the s-wave scattering properties is a soft disk of radius a,

$$V(r) = V_0\Theta(R-a). \tag{C1}$$

We are particularly interested in the case $V_0<0$, corresponding to an attractive disk.

The s-wave phase shift δ_0 for the soft disk potential is determined by continuity of the logarithmic derivative of the wave function at $r=a$:

$$\tan\delta_0 = \frac{qJ_0(ka)J_1(qa) - kJ_1(ka)J_0(qa)}{qY_0(ka)J_1(qa) - kY_1(ka)J_0(qa)}, \tag{C2}$$

where

$$q \equiv \sqrt{2(E-V_0)}$$

is the wave number inside the disk.

Having calculated the s-wave phase shift, it is straightforward to confirm that we can simulate the s-wave scattering from a soft attractive disk with a t matrix:

$$s(k) = \frac{-2\tan\delta_0}{1 - i\tan\delta_0}. \tag{C3}$$

The negative energy poles of the t matrix in Eq. (C3) occur at

$$qK_0(\kappa a)J_1(qa) = \kappa K_1(\kappa a)J_0(qa), \tag{C4}$$

where $\kappa\equiv\sqrt{-2E}$. Equation (C4) can easily be shown to be the characteristic equation for bound states of the 2D cylindrical well.

[1] S. Fan and J. D. Joannopoulos, Phys. Rev. B **65**, 235112 (2002).
[2] A. Calzolari, C. Cavazzoni, and M. Buongiorno-Nardelli, Phys. Rev. Lett. **93**, 096404 (2004).
[3] T. M. Wallis, N. Nilius, and W. Ho, Phys. Rev. Lett. **89**, 236802 (2002).
[4] J. N. Crain and D. T. Pierce, Science **307**, 703 (2005).
[5] J. S. Hersch and E. J. Heller, Phys. Rev. Lett. **81**, 3059 (1998).
[6] E. J. Heller, Phys. Rev. Lett. **77**, 4122 (1996).
[7] M. G. E. da Luz, A. S. Lupu-Sax, and E. J. Heller, Phys. Rev. E **56**, 2496 (1997).
[8] L. L. Foldy, Phys. Rev. **67**, 107 (1945).
[9] L. S. Rodberg and R. B. Thaler, *Introduction to the Quantum Theory of Scattering* (Academic, New York, 1967).
[10] J. Korringa, Physica (Amsterdam) **13**, 392 (1947).
[11] W. Kohn and N. Rostoker, Phys. Rev. **94**, 1111 (1954).
[12] Z. Liu, C. T. Chan, P. Sheng, A. L. Goertzen, and J. H. Page, Phys. Rev. B **62**, 2446 (2000).
[13] J. Y. Vaishnav, A. Itsara, and E. J. Heller, Phys. Rev. B **73**, 115331 (2006).
[14] M. G. Moore, T. Bergeman, and M. Olshanii, J. Phys. IV **116**, 69 (2004).
[15] J. E. Lennard-Jones and A. F. Devonshire, Proc. R. Soc. London, Ser. A **156**, 6 (1936).
[16] R. Parker, J. Sound Vib. **5**, 330 (1967).
[17] D. V. Evans and C. M. Linton, Q. J. Mech. Appl. Math. **46**, 643 (1993).
[18] A. Sommerfeld, *Optics* (Academic Press, New York, 1954).
[19] C. M. Linton and P. A. Martin, SIAM J. Appl. Math. **64**, 1035 (2004).

[20] M. F. Crommie, C. P. Lutz, and D. M. Eigler, Science **262**, 218 (1993).
[21] G. A. Fiete and E. J. Heller, Rev. Mod. Phys. **75**, 933 (2003).
[22] Y. S. Chan, Ph.D. thesis, Harvard University, 1997.
[23] M. F. Crommie, C. P. Lutz, D. M. Eigler, and E. J. Heller, Physica D **83**, 90 (1995).
[24] J. D. Walls, J. Huang, R. M. Westervelt, and E. J. Heller, Phys. Rev. B **73**, 035325 (2006).
[25] N. A. Nicorovici, R. C. McPhedran, and R. Petit, Phys. Rev. E **49**, 4563 (1994).
[26] J. S. Hersch, Ph.D. thesis, Harvard University, 1999.